J. Fluid Mech. (1977), *vol.* 83, *part* 1, *pp.* 119–127
Printed in Great Britain

Waves on water jets

By J. W. HOYT
U. S. Naval Academy, Annapolis, Maryland 21402
AND J. J. TAYLOR
Naval Ocean Systems Center, San Diego, California 92152

(Received 31 March 1977)

By the use of high-speed photography, instabilities occurring in high Reynolds number water jets discharging into air have been made visible. These instabilities include the axisymmetric mode accompanying the transition from laminar to turbulent flow at the nozzle exit, spray formation as a culmination of the axisymmetric disturbances, and, further downstream, helical disturbances which result in the entire jet assuming a helical form. The final disruption of the jet is due to amplification of the helical waves. It is further shown that the amplification of the helical disturbances is due in part to aerodynamic form drag, since jets discharging into surrounding air moving at the same speed as the jet remain relatively stable, compared with the case when the jet is discharged into stagnant air.

1. Introduction

This study of waves and instabilities on water jets has been influenced by the remarkable change in the past decade in the general approach to problems of shear-flow instability. Large-scale structure is now recognized in many types of shear flow previously thought to be of a random, chaotic nature exclusively. Large-scale structures in air jets, for example, have been studied recently by Lau & Fisher (1975) and Lee (1976). Excellent reviews of organized structure in turbulent shear flows have been given by Roshko (1976) and Laufer (1975).

Stability studies of low-speed laminar jets have a long history, dating back to Rayleigh and beyond. These have been competently reviewed by Miesse (1955), Chandrasekhar (1961), Chen & Davis (1964), Grant & Middleman (1966) and most recently by McCarthy & Molloy (1974). The stability theories covered in these reviews apply to low-speed jets, their axisymmetric 'varicose' instabilities and their breakup into discrete sections or drops having sizes comparable to the jet diameter. As the jet speed increases, these theories of stability begin to give a poor prediction for, say, the jet breakup length.

In terms of radial spreading of high-speed jets, even less success has been obtained theoretically, and standard texts on jets (Birkoff & Zarantonello 1957; Abramovich 1963) rely on empirically derived 'spreading angles' to compute the dispersion of a jet.

Batchelor & Gill (1962) noticed that in the linearized equation of motion the components

$$u_x, u_\phi \sim \exp[in\phi + i\alpha(x-ct)]$$

of the disturbance velocity differ in phase by $\frac{1}{2}\pi$ from the component

$$u_r \sim i\exp[in\phi + i\alpha(x-ct)],$$

where x, r and ϕ are cylindrical co-ordinates, α is the wavenumber and c_i determines the stability of the jet. Thus when $n = 1$ a helical instability is predicted as compared with the axisymmetric instability for $n = 0$. Batchelor & Gill went on to show, using temporal instability analysis, that in the far-downstream region of the jet only the helical modes are amplified.

Mattingly & Chang (1974) extended the analysis of Batchelor & Gill by making a spatial instability study of the same equations. A spatial instability analysis considers the disturbances to oscillate in time and space, but dampen or amplify exponentially in space. For this type of analysis, then, the wavenumber α is considered complex, its imaginary part indicating growth or decay of disturbances with x. The frequency c is considered real.

The results of the analysis depend somewhat on the jet velocity profile selected, and Mattingly & Chang used an experimentally determined jet velocity profile to evaluate the stability equations numerically. Their evaluation showed that the axially symmetric disturbances had greatest amplification in the first three diameters of the jet, being superseded in amplification rate by the helical disturbances which predominate downstream from there.

Brennen (1970) made a spatial stability analysis of the waves on cavity flows, using a two-dimensional boundary-layer model, and evaluated the Orr–Sommerfield equation numerically to yield the preferred frequency for amplified waves on the surface of the cavity. The computed frequency was close to that actually observed on a water–cavity interface.

In the present work, photography was used to study the various waves on the surface of high-speed water jets. In addition, the local velocity of the air into which the jet was discharged was varied in order to determine the effect of air resistance on the instability pattern of the jet.

The effect of air resistance on the stability and breakup length of jets has not been well defined; Phinney (1975) found that variation of the density of the surrounding air over a substantial range had no effect on the breakup length of a turbulent water jet. Davies & Young-Hoon (1974) saw no effect of air pressure on the jet appearance. On the other hand, Fenn & Middleman (1969) found no effect of air density on low viscosity (water-like) laminar jets, but a rather considerable effect on jets of viscous liquids, with lowered air density leading to longer jet travel before breakup. In the present work, rather than varying the density ρ_A of the air into which the water jets were injected, the relative air velocity could be varied from co-flowing to counter-flowing. Thus the effect of the relative air velocity V_r on the air-drag on the water jet (proportional to $\rho_A V_r^2$) could be evaluated.

2. Experimental

A sketch of the experimental apparatus is given in figure 1, where it can be seen that a coaxial air stream is arranged to surround the water-jet inlet piping and nozzle and proceed, in ducting, to the photography station. By interchanging the inlet and outlet blower connexions, air could be drawn from the region surrounding the jet in a direction opposite to the jet flow. The blower speed was varied by an adjustable transformer. The air inlet to the test section consisted of a scroll volute, taken from another blower, together with transitions and a honeycomb section to provide axial

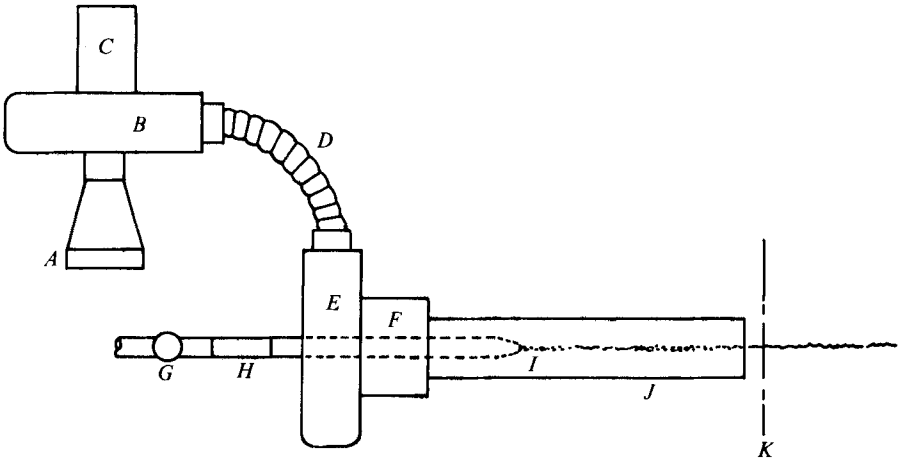

FIGURE 1. Sketch of experimental apparatus. *A*, anemometer; *B*, blower; *C*, variable speed motor; *D*, flexible hose; *E*, inlet volute; *F*, air-straightening honeycomb; *G*, inlet water-pressure gauge; *H*, water-straightening honeycomb; *I*, water nozzle; *J*, typical air-enclosure tube; *K*, typical centre-line of camera lens.

air flow evenly distributed around the jet. Air velocities were computed by noting the calibrated anemometer reading, which gave the air volume flow in ft^3/min. Maximum air velocities around the jet in either direction were of the order of 120 ft/s. The water jet was operated at a constant nozzle base pressure of 60 $lb/in.^2$, leading to a computed jet exit velocity of 90 ft/s, a value which could be checked by the internal mechanism of the image-compensating camera. The Reynolds number based on jet speed and diameter was thus about 10^5.

The water-jet nozzle diameter was 0·125 in.; the internal contours consisted of an initial 30° conical approach followed by a transition to 15° convergence to a constant-diameter section two diameters long. All internal contours were faired together. A honeycomb section in the nozzle inlet piping provided a flow-straightening effect.

A separate ducting tube varying only in length was provided for the air at each photography station, so that a smooth internal surface was preserved. For photography next to the nozzle, optical windows were provided on either side of the tube to permit lighting and photography; for stations further out in the stream, the tube was extended to within 1 in. of the centre-line of the camera lens.

Another series of photographs was taken with a larger nozzle discharging into stagnant air. Here the jet diameter was 0·25 in.; at a nozzle base pressure of 50 $lb/in.^2$ the jet speed was measured to be 83 ft/s and the Reynolds number was about 2×10^5. This nozzle was a simple cone with a 7° half-angle followed by a one-diameter parallel section.

The photography, being crucial to the investigation, was accomplished with specially designed cameras and lighting to furnish the maximum detail. Since the jet motion is predominantly axial, a camera can be designed to compensate for this motion (i.e. hold the image relatively stationary on the film) by either moving the film in the opposite axial direction as it is exposed (Taylor 1975) or by swinging the image with a rotating mirror so that the image is momentarily stationary in the film plane. Both methods were used in this study. Of course the primary exposure control

is a short duration flash, but the image-compensation technique yields appreciably better definition than relying on a flash alone to stop the jet motion.

Photographs of the jet discharging into stagnant air were taken with the moving-film camera as described previously (Hoyt, Taylor & Runge 1974). Those photographs were taken on $2\frac{1}{4} \times 3\frac{1}{4}$ in. Tri-X cut film. For the jets discharging into flowing air streams, a new rotating-mirror camera provided image-motion compensation, allowing Tri-X, ASA320 roll film to be used. At the instant the motion-compensated image appears in the film plane, an 8 μs electronic flash is actuated. Through a system of mirrors, the flash illumination is directed onto both the top and the bottom of the jet, which is back-lighted at 45° from the horizontal. The jet is shielded from ambient light so that the flash is dominant, and the image thus appears brightly illuminated against a black background. A magnification of approximately 2·6 is achieved in the camera; higher magnifications were used in the study of spray formation, at the expense of loss of depth of field in the image.

3. Results

The photographs from the jet discharging into stagnant air will be described first. Figure 2 (plate 1) shows the jet emerging from the nozzle and the initial few diameters of travel. Owing to the high area contraction ratio in the nozzle (42), the flow leaving the nozzle is laminar, even though the inflow to the nozzle is turbulent. Relaminarization in nozzles with high contraction ratios is well documented for air flow (Back, Cuffel & Massier 1969; Romjee & Hussain 1976) and need not be discussed further here. Axisymmetric instability waves are immediately apparent after less than one diameter of air travel. These instabilities are further amplified in the next, rather chaotic region and culminate in the ejection of spray droplets. Further discussion of the spray-ejection zone will follow later.

Figure 3 (plates 2 and 3) traces the jet path by means of photos taken every 24 nozzle diameters until a station 216 diameters downstream was reached. Axisymmetric instabilities do not seem to appear on the jet surface after the initial spray-formation zone (10 nozzle diameters or so). Instead, instabilities begin to bend the jet into a helical path, first perceptible at about 70 diameters and clearly evident by 100 diameters and further downstream. Honeycomb flow straighteners were placed in the nozzle inlet piping, and considerable auxiliary experimentation was carried out to assure that the helical shape was not the result of swirl in the inlet piping or some other experimental artifact. The helix gradually increases in average pitch with increasing jet length.

Turning next to the effect of the velocity of the surrounding air on the jet, figure 4 (plate 4) shows the jet at 238 diameters downstream from the nozzle. At this distance from the nozzle the jet has almost lost continuity in low-speed or stagnant surrounding air (figure 4*a*). As the air velocity is progressively increased (figures 4*b*–*d*) the jet becomes much more stable and finally becomes almost rod-like as the air velocity approaches and exceeds that of the water. The helical-wave instability is still present, but only a small fraction of the width excursion remains. All of the photos in figure 4 were taken within a few minutes of each other, so that upstream water-jet conditions were unchanged; the water nozzle pressure was set at a constant value while the air velocity was varied.

Figure 5 (plates 5 and 6) depicts the effect of air velocity at a point 104 diameters from the exit of the water nozzle. Figure 5(*a*) shows the rod-like jet produced when the air velocity slightly exceeds that of the water. As the air velocity is decreased (figures 5*b–d*), the jet becomes more and more unstable. When the air velocity is reversed with respect to the water jet as in figures 5(*e*)–(*h*), the jet continues to become less stable until in figure 5(*h*), with a reverse air speed about equal to the jet speed, the jet has almost blown apart. The mode of instability remains helical in all cases, and the amplitude of the instabilities increases with increasing velocity of the air relative to the jet (i.e. $V_r = V_{\text{air}} - V_{\text{jet}}$). The wavenumber of the instability does not seem to change appreciably with V_r.

The effect of air velocity on the axisymmetric disturbances was investigated by taking photographs next to the nozzle. No effect of air velocity whatsoever can be detected. Figure 6 (plate 7) shows the first eight diameters of travel. Thus the mechanism of initial spray-droplet formation seems to be relatively unaffected by relative air velocity compared with the helical instability phase further downstream. Since the spray-formation phase appears to follow from the axisymmetric instability and neither is modified by relative air velocity, a further series of photos was taken at higher magnification with the jet discharging into stagnant air. Figure 7 (plate 8) is a representative selection of scenes of the spray-formation mode, taken three diameters downstream from the nozzle exit. Events are extremely rapid in this area and no two scenes are alike. The underlying mechanism of the spray-droplet ejection from the body of the jet seems to be amplification of the axisymmetric disturbances on the jet surface as can be inferred from the scenes in figure 8 (plate 9). The photographic technique does not allow us to determine whether the axisymmetric disturbances and the spray-formation events move with the jet surface velocity or at some other speed.

As a further indication of the effect of air resistance on the various instabilities, the nozzle tests discharging into stagnant air were repeated using instead of water a 200 p.p.m. solution of poly(ethylene oxide), which is a viscoelastic liquid and thus tends to damp disturbances more readily than purely viscous fluids. As shown in figure 9 (plates 10 and 11), the axially symmetric disturbances are greatly suppressed, and the spray-formation mode is eliminated. Whether this is due to viscoelasticity or to transition to turbulence inside the nozzle is not clear, but what is evident is that the helical disturbances are not damped, but show the same amplification as in the pure water jet. This is an indication, then, of the important role played by air resistance in the eventual disruption and breakup of the jet.

4. Discussion

The complex system of disturbances occurring on the surface of a water jet discharging into air can be described as 'axially symmetric' or 'helical' in only a rather loose sense. However, the initial system of waves which accomplish the transition from laminar to turbulent flow on the surface of the jet can be regarded as almost axisymmetric. On applying Mattingly & Chang's (1974) theory and numerical evaluation and non-dimensionalizing the wavelength by half the thickness of the laminar boundary layer, estimated to begin at the parallel section of the nozzle, a dimensional wavelength λ' of 0·025 in. is estimated for the waves accompanying

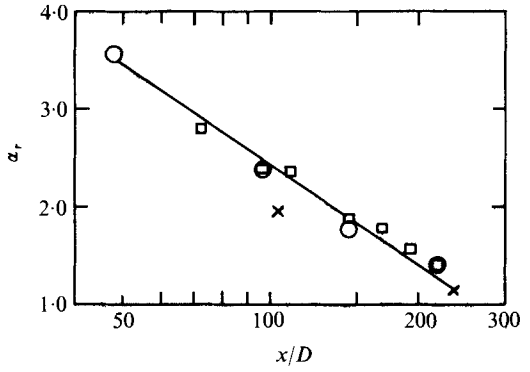

FIGURE 10. Wavenumber $\alpha_r = \pi D/\lambda$ measured from photographs as a function of downstream distance x/D. ○, 0·25 in. diameter nozzle, polymer solution; □, 0·25 in. diameter nozzle, water; ×, 0·125 in. diameter nozzle, water.

transition. This is based on the numerical value of $\alpha_r = 0{\cdot}411$ in Mattingly & Chang for a station near the nozzle exit, at $x/D = 0{\cdot}125$. By measuring enlarged photos of the waves, a value of 0·018 in. is obtained as the average value from nine different photos. Considering the assumptions made about boundary-layer growth in the nozzle, the agreement between theory and experiment is good.

The agreement is also good with Brennen's (1970) two-dimensional stability analysis, which predicts a wavelength of 0·17 in. for the most highly amplified disturbance. Agreement is also excellent between the non-dimensional distance from the nozzle end to the first appearance of turbulent flow and a similar measurement made by Brennen of the length of cavity flow before turbulent breakup of the waves on a cavity surface (Hoyt & Taylor 1976). Brennen found an e^8 relationship between the body-surface roughness and the amplitude of the cavity waves just before turbulent breakup; a similar relationship between the nozzle-surface roughness and the axisymmetric wave amplitude before turbulence appears on the jet surface may be expected.

For the $n = 1$ helical instabilities, no corresponding experimental results could be located in the literature except a photograph in the review by Roshko (1976) of an air jet exhibiting helical structure far downstream from the nozzle. Batchelor & Gill (1962) predict that the downstream jet is unstable only to the $n = 1$ helical disturbances and that the axial wavelength is 'larger than some critical value several times the jet diameter'. While it is recognized that the present experiments were conducted in a Reynolds number and disturbance size range far above that contemplated in the theoretical development, the general trends outlined by inviscid theory seem to apply. The photographs of the jet flow (figure 3) show that the initially visible helical form of the jet has wavelengths of the order of a jet diameter or less, but the axial wavelength increases with x until it is certainly several diameters before the jet disintegrates. Figure 10 shows the measured wavenumber, with λ non-dimensionalized by $\frac{1}{2}D$, as a function of the non-dimensional axial length of jet from the nozzle. Data from all the experiments seem to correlate reasonably well for both jet diameters, and regardless of the presence of polymer in the water.

Turning now to the amplitude of the helical disturbances, we see immediately from figures 4 and 5 that this is entirely a function of the velocity of the surrounding

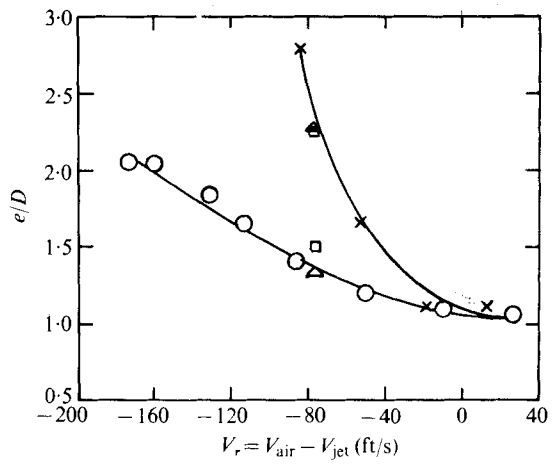

FIGURE 11. Excursion of jet e over nozzle diameter D as a function of air velocity relative to the water jet. x/D: ○, 104; ×, 238 (D = 0·125 in., water); △, 104, 238 (D = 0·25 in., water); □, 104, 238 (D = 0·25 in., polymer solution).

air into which the water jet is discharged. The photographs in figures 4 and 5 thus show the overwhelming effect of air resistance on jet breakup. Contrary to previous work, which showed little or no effect of the density of the surrounding air on jet breakup, the velocity of the air surrounding the jet makes a major contribution to jet stability. If the maximum jet width e shown in the scenes of figures 4 and 5, divided by the nozzle diameter D, is plotted as a function of the velocity of the air relative to the jet (i.e. $V_r = V_{air} - V_{jet}$), the curves shown in figure 11 as a function of x/D are obtained. Additional points from figures 3 and 9 are included.

We thus see that the mechanism of jet breakup must be related to the relative air velocity and thus to the drag on the perturbed jet. As the relative air velocity tends to zero, the jet diameter tends to that of the nozzle. Hence it is necessary to decide whether the effect is related to the viscous drag $c_f(\frac{1}{2}\rho V^2 S)$, where S is the exposed surface area of the jet, or to the form drag $c_D(\frac{1}{2}\rho V^2 A)$, where A is the frontal area of the jet helix.

The question is decided by operating the jet with a much smoother jet surface as in figure 9 so that the roughness-based friction coefficient c_f is greatly reduced. As can be seen from figures 10 and 11, the helical excursions and wavenumbers are unaffected by the smoothing effect of the polymers on the viscous drag. Thus the mechanism of jet breakup appears to be form drag on the helical components of the jet. This then offers an explanation of why jets from fire hoses and fountains break up, a phenomenon people have wondered about for centuries. The inherent instabilities, amplified from infinitesimal disturbances, are further amplified in the downstream section of the jet by air resistance of the form-drag type.

A further confirmation of the form-drag resistance amplification of downstream disturbances comes from considering the near-nozzle flow field, which is affected primarily by the $n = 0$ axially symmetric disturbances. As shown in figure 6, no discernible effect of relative air velocity on the axially symmetric disturbances or the spray-formation mode can be seen. If viscous air resistance were an important disrupting mechanism, one should see an effect here. The initial spray-detachment mechanism

seems to be entirely separate from the air resistance effect. As shown in figures 7 and 8, spray detachment seems more a matter of amplified wave motion than outside environment, and appears to be a culmination of the amplified axisymmetric disturbances accompanying the transition from laminar to turbulent flow on the surface of the jet emerging from the nozzle. Ejecta from the vertical motion in the loops of the waves are tied briefly to the mainstream by a water filament which pinches off owing to surface tension, forming the spray droplets. The above mechanism is thus insensitive to the velocity of the surrounding air as discussed previously.

5. Concluding remarks

The waves on these high Reynolds number jets show a remarkable similarity to the instabilities predicted from inviscid stability theory, even though the jets are operating far outside the range of linear theory. The important amplifying effect of air resistance on the helical instabilities of water jets shows that this is the primary mechanism of jet breakup in high-speed jets. A useful future task will be to measure the wave speed of the various instabilities, compared with the bulk speed of the jet.

The experimental work was performed at the Naval Ocean Systems Center with the support of the Office of Naval Research. Analysis of the results was carried out during a Naval Sea Systems Command Research Professorship at the U.S. Naval Academy.

REFERENCES

ABRAMOVICH, G. N. 1963 *The Theory of Turbulent Jets*. M.I.T. Press.

BATCHELOR, G. K. & GILL, A. E. 1962 Analysis of the stability of axisymmetric jets. *J. Fluid Mech.* **14**, 529.

BACK, L. H., CUFFEL, R. F. & MASSIER, P. F. 1969 Laminarization of a turbulent boundary layer in nozzle flow. *A.I.A.A. J.* **7**, 730.

BIRKHOFF, G. & ZARANTONELLO, E. H. 1957 *Jets, Wakes, and Cavities*. Academic Press.

BRENNEN, C. 1970 Cavity surface wave patterns and general appearance. *J. Fluid Mech.* **44**, 33.

CHANDRASEKHAR, S. 1961 *Hydrodynamic and Hydromagnetic Stability*. Oxford: Clarendon Press.

CHEN, T.-F. & DAVIS, J. R. 1964 Disintegration of a turbulent water jet. *A.S.C.E. Proc.* **90**, 175.

DAVIES, J. T. & YOUNG-HOON, A. A. 1974 Restrained turbulent jets of a non-Newtonian solution. *Chem. Engng Sci.* **29**, 1115.

FENN, R. W. & MIDDLEMAN, S. 1969 Newtonian jet stability: the role of air resistance. *A.I.Ch.E. J.* **15**, 379.

GRANT, R. P. & MIDDLEMAN, S. 1966 Newtonian jet stability. *A.I.Ch.E. J.* **12**, 669.

HOYT, J. W. & TAYLOR, J. J. 1976 Turbulence structure in a water jet discharging in air. *Proc. IUTAM Conf. Turbulence and Drag Reduction, Washington*. To appear as *Phys. Fluids Suppl.*

HOYT, J. W., TAYLOR, J. J. & RUNGE, C. D. 1974 The structure of jets of water and polymer solution in air. *J. Fluid Mech.* **63**, 635.

LAU, J. C. & FISHER, M. J. 1975 The vortex-street structure of turbulent jets. Part 1. *J. Fluid Mech.* **67**, 299.

LAUFER, J. 1975 New trends in experimental turbulence research. *Ann. Rev. Fluid Mech.* **7**, 307.

LEE, B. H. K. 1976 Some measurements of spatial instability waves in a round jet. *A.I.A.A. J.* **14**, 348.

MCCARTHY, M. J. & MOLLOY, N. A. 1974 Review of stability of liquid jets and the influence of nozzle design. *Chem. Engng J.* **7**, 1.

MATTINGLY, G. E. & CHANG, C. C. 1974 Unstable waves on an axisymmetric jet column. *J. Fluid Mech.* **65**, 541.

MIESSE, C. C. 1955 Correlation of experimental data on the disintegration of liquid jets. *Ind. Engng Chem.* **47**, 1690.

PHINNEY, R. E. 1975 Breakup of a turbulent liquid jet in a low pressure atmosphere. *A.I.Ch.E. J.* **21**, 996.

ROMJEE, V. & HUSSAIN, A. K. M. F. 1976 Influence of the axisymmetric contraction ratio on free-surface turbulence. *A.S.M.E. J. Fluids Engng* **198**, 506.

ROSHKO, A. 1976 Structure of turbulent shear flows: a new look. *A.I.A.A. J.* **14**, 1349.

TAYLOR, J. J. 1975 Camera apparatus for making photographic images on moving cut film pieces. *U.S. Patent* no. 3.925.796.

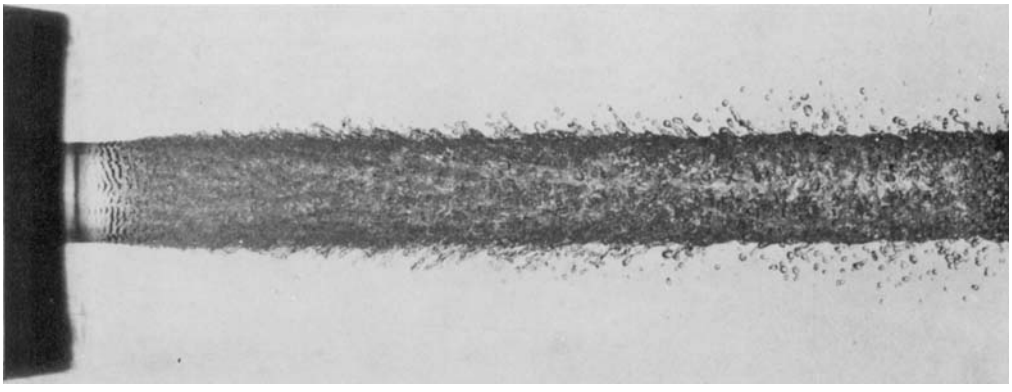

FIGURE 2. Jet emerging from 0·25 in. diameter nozzle into stagnant air.
Jet velocity = 83 ft/s.

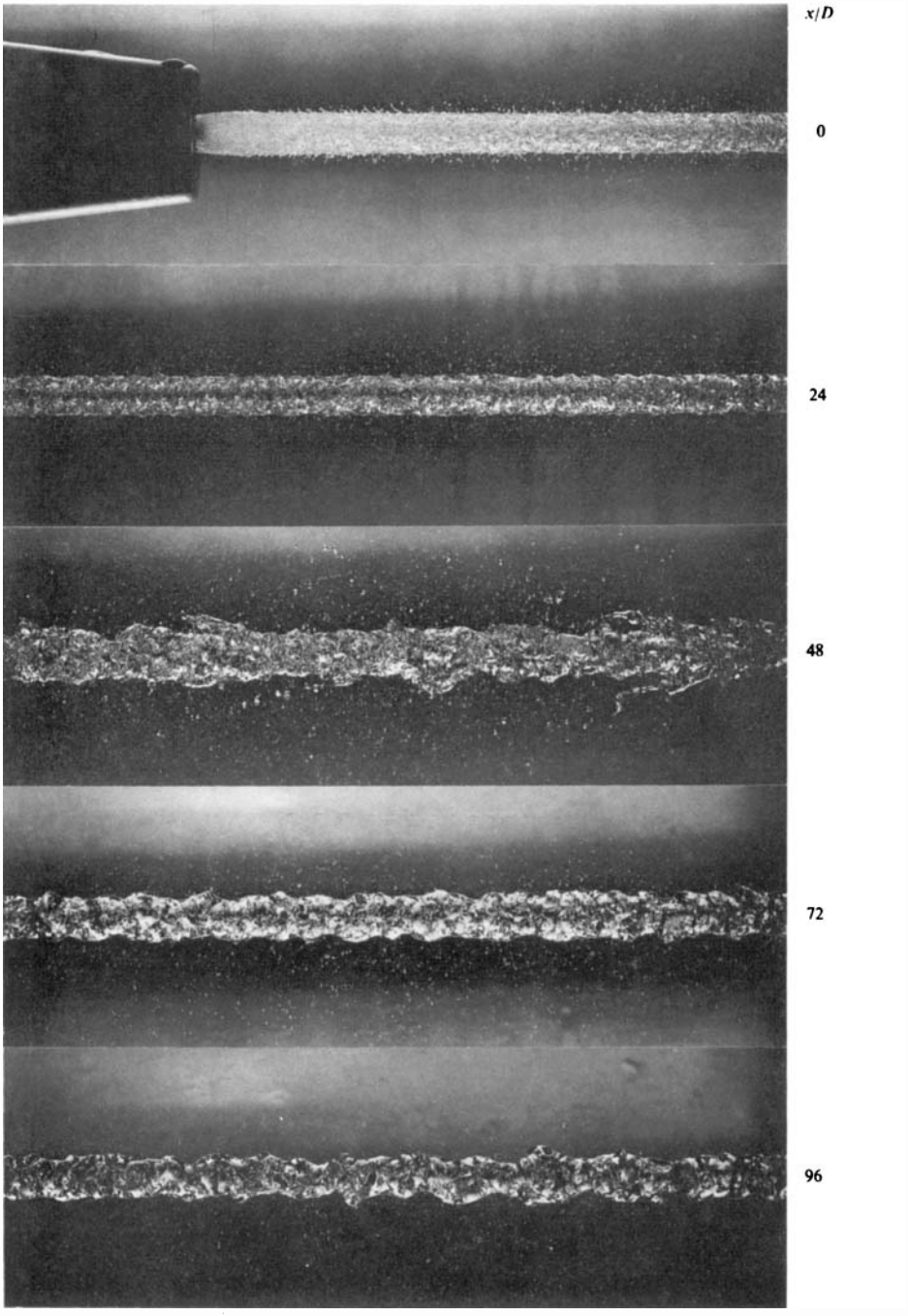

FIGURE 3 (*a*). For legend see facing page.

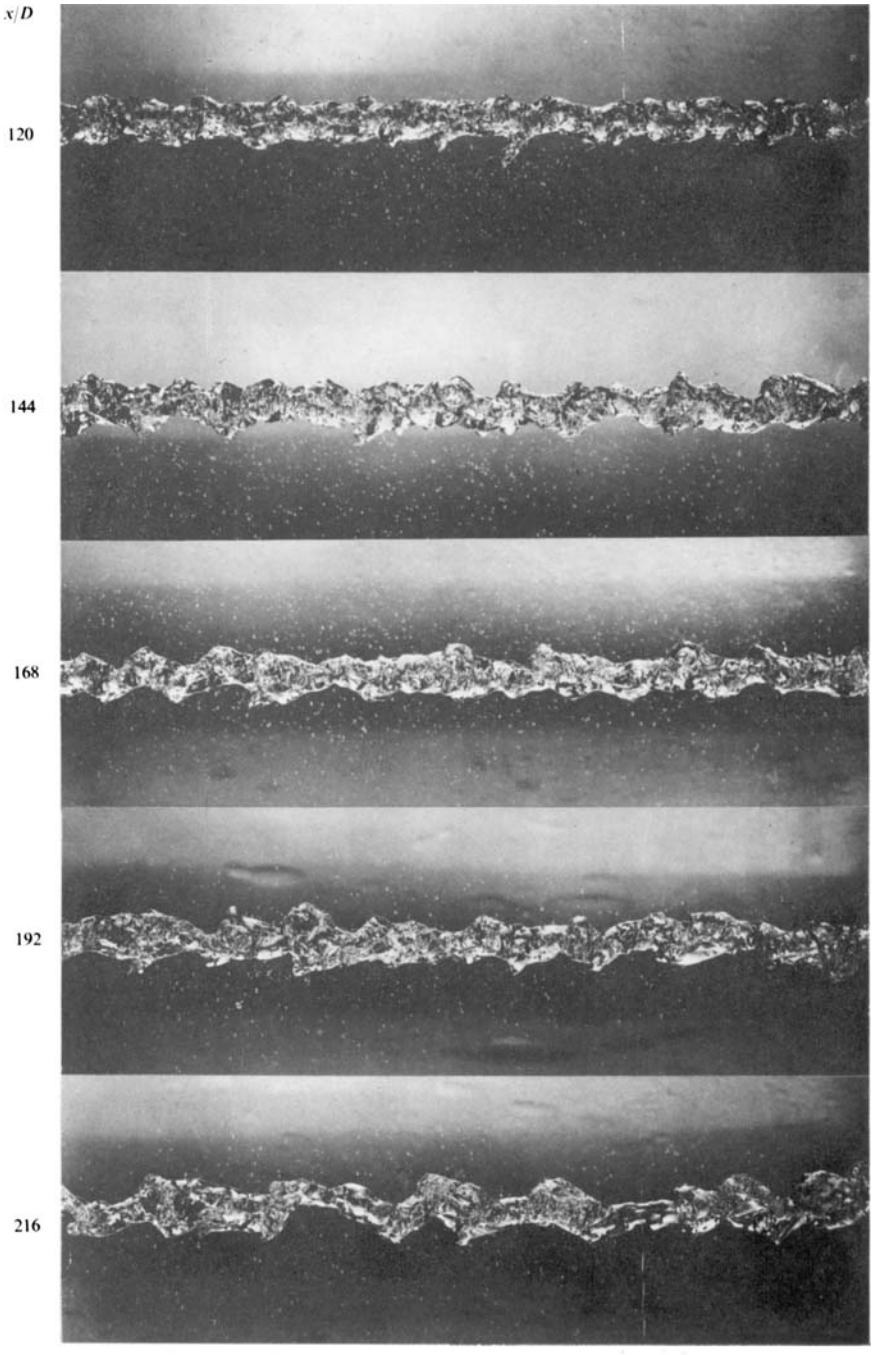

(*b*)

FIGURE 3. Photos of jet from 0·25 in. diameter nozzle in stagnant air; photos were taken 24 nozzle diameters apart.

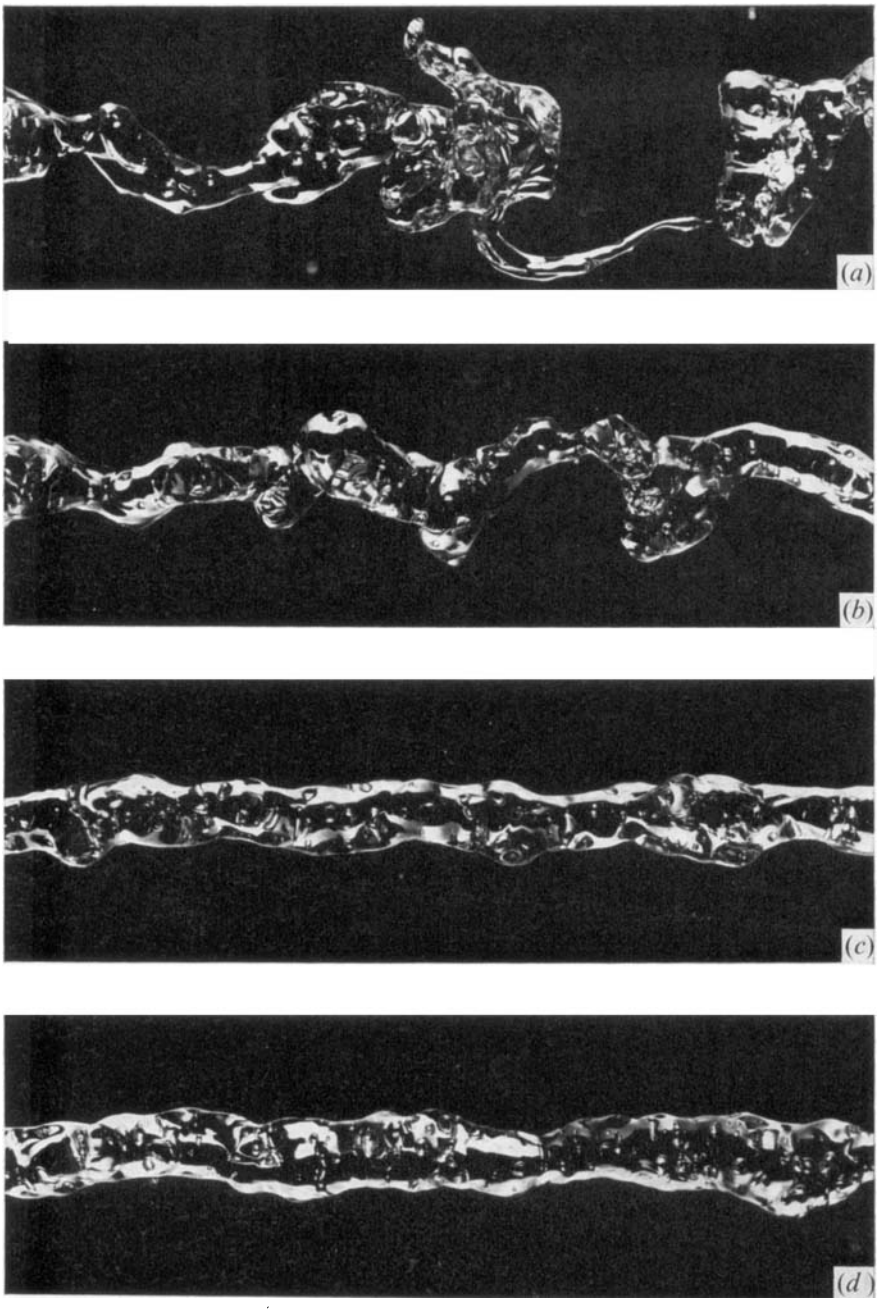

FIGURE 4. Appearance of jet from 0·125 in. diameter nozzle at $x/D = 238$. Air velocity (ft/s): (*a*) 7; (*b*) 36; (*c*) 72; (*d*) 103. Flow from left to right. Jet velocity at nozzle = 90 ft/s.

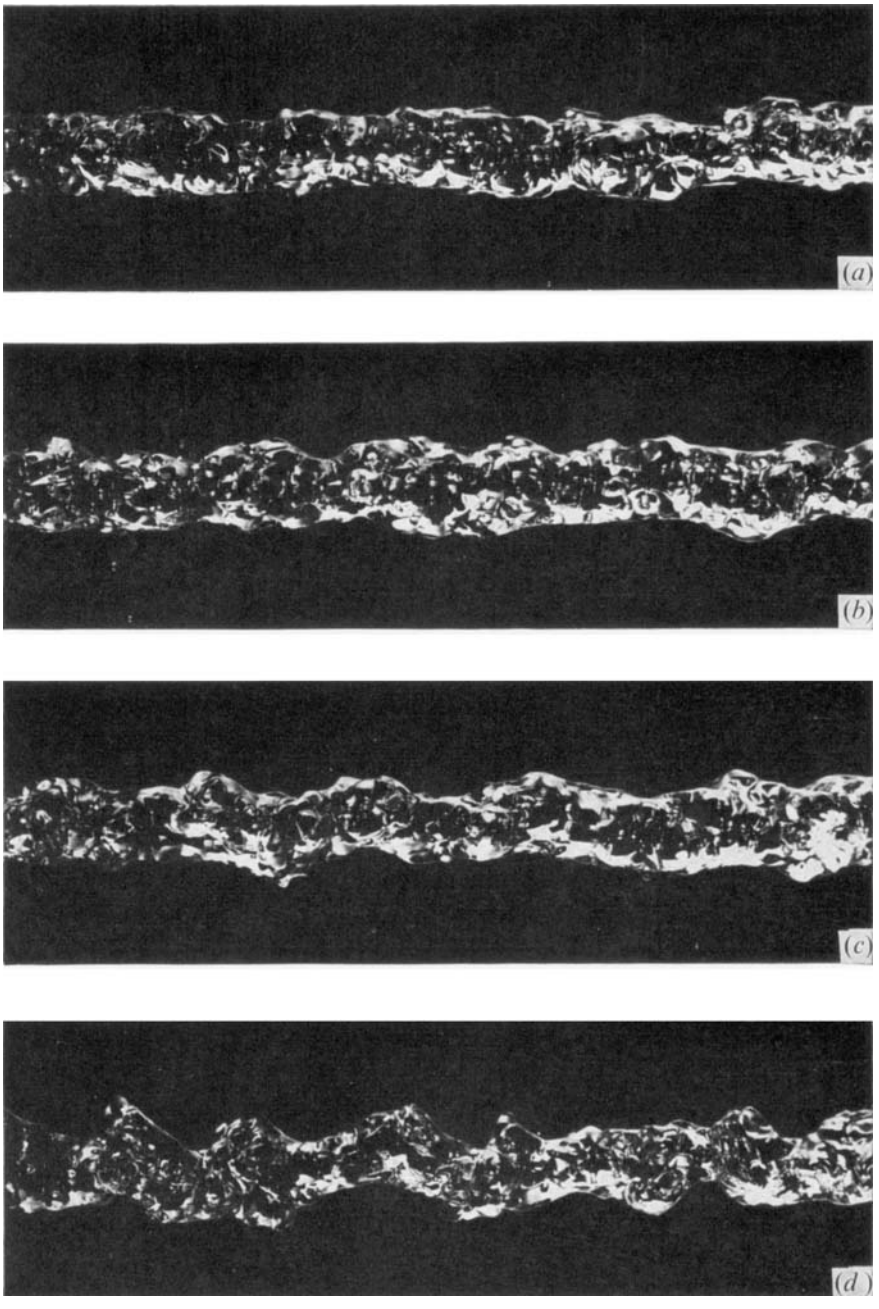

FIGURES 5 (*a–d*). For legend see next page.

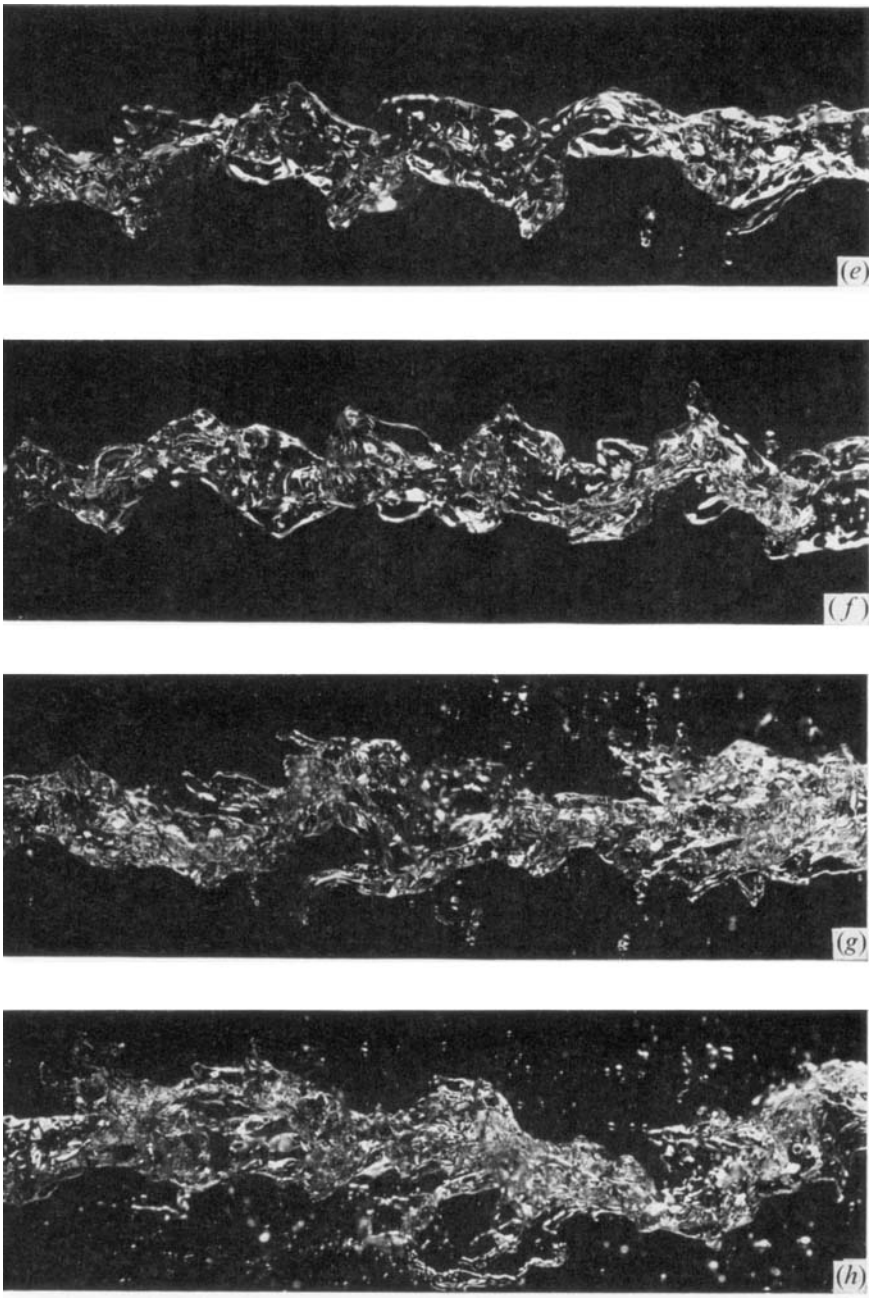

FIGURE 5. Appearance of jet from 0·125 in. diameter nozzle at $x/D = 104$. Air velocity from left to right (ft/s): (*a*) 116; (*b*) 80; (*c*) 40; (*d*) 4·8; (*e*) −23; (*f*) −40; (*g*) −70; (*h*) −83. Water flow from left to right. Jet velocity at nozzle = 90 ft/s.

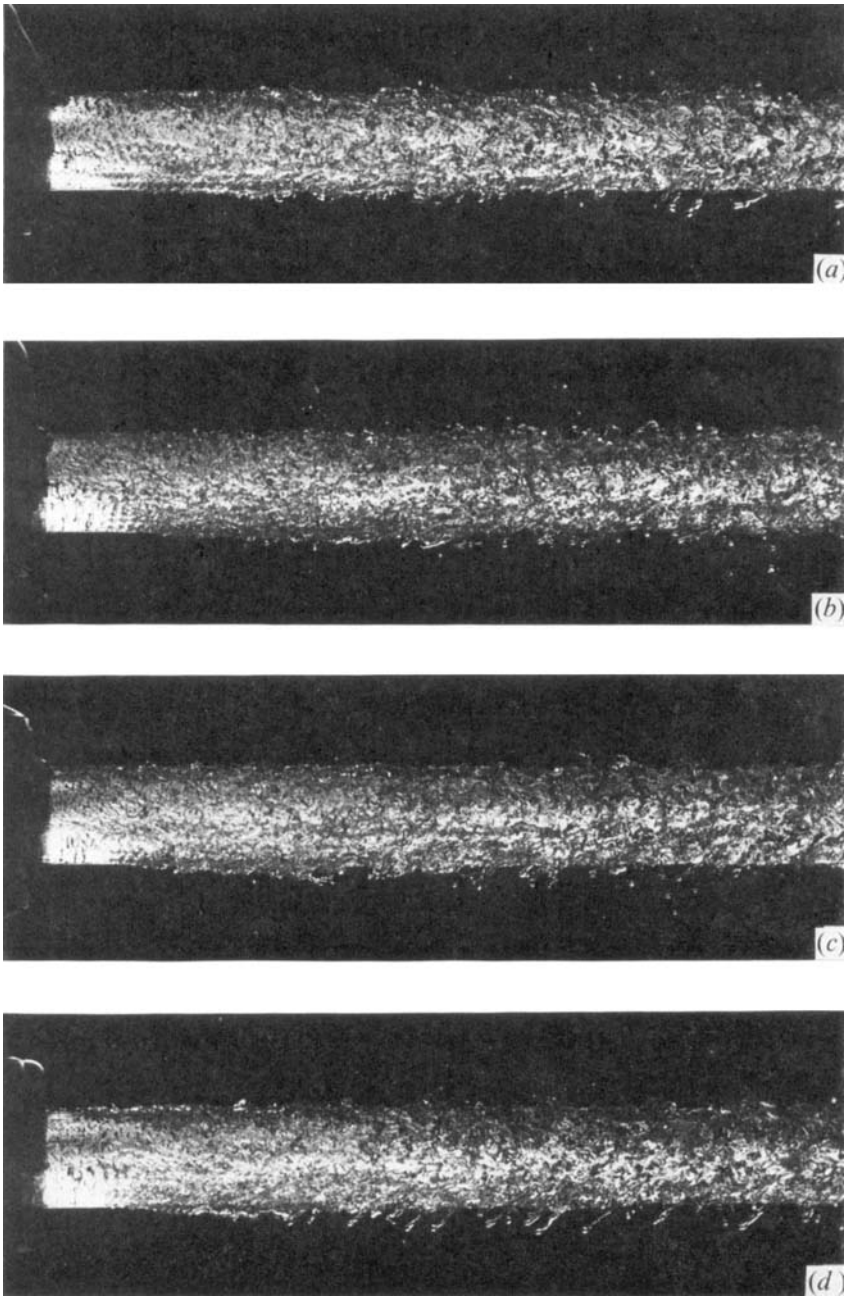

FIGURE 6. Appearance of 0·125 in. diameter water jet at nozzle exit. Air velocity (ft/s): (*a*) 119; (*b*) 80; (*c*) 0; (*d*) −80. Jet velocity = 90 ft/s.

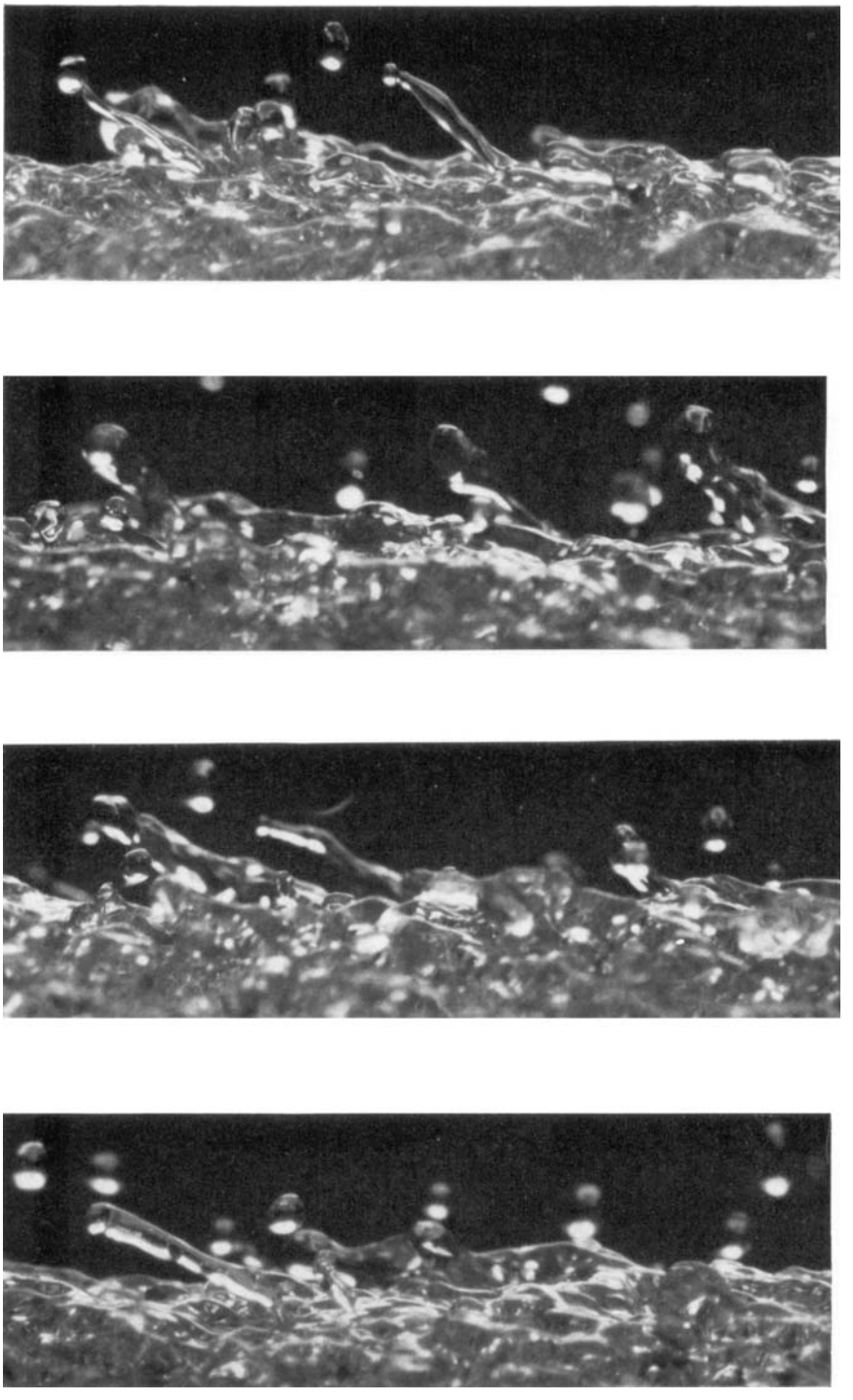

FIGURE 7. Typical scenes of spray formation near the 0·125 in. diameter nozzle at zero air velocity and a jet velocity of 83 ft/s.

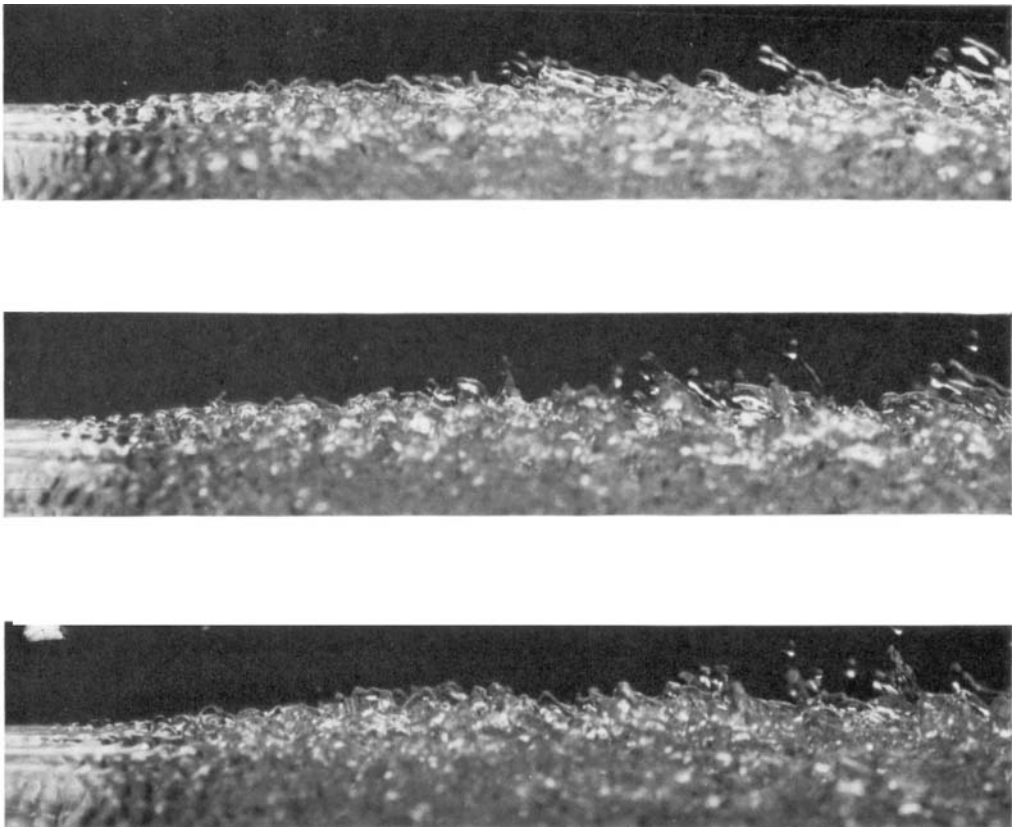

FIGURE 8. Typical scenes of amplified wave breakup and spray ejection at zero air velocity for the 0·25 in. diameter nozzle at a jet velocity of 83 ft/s.

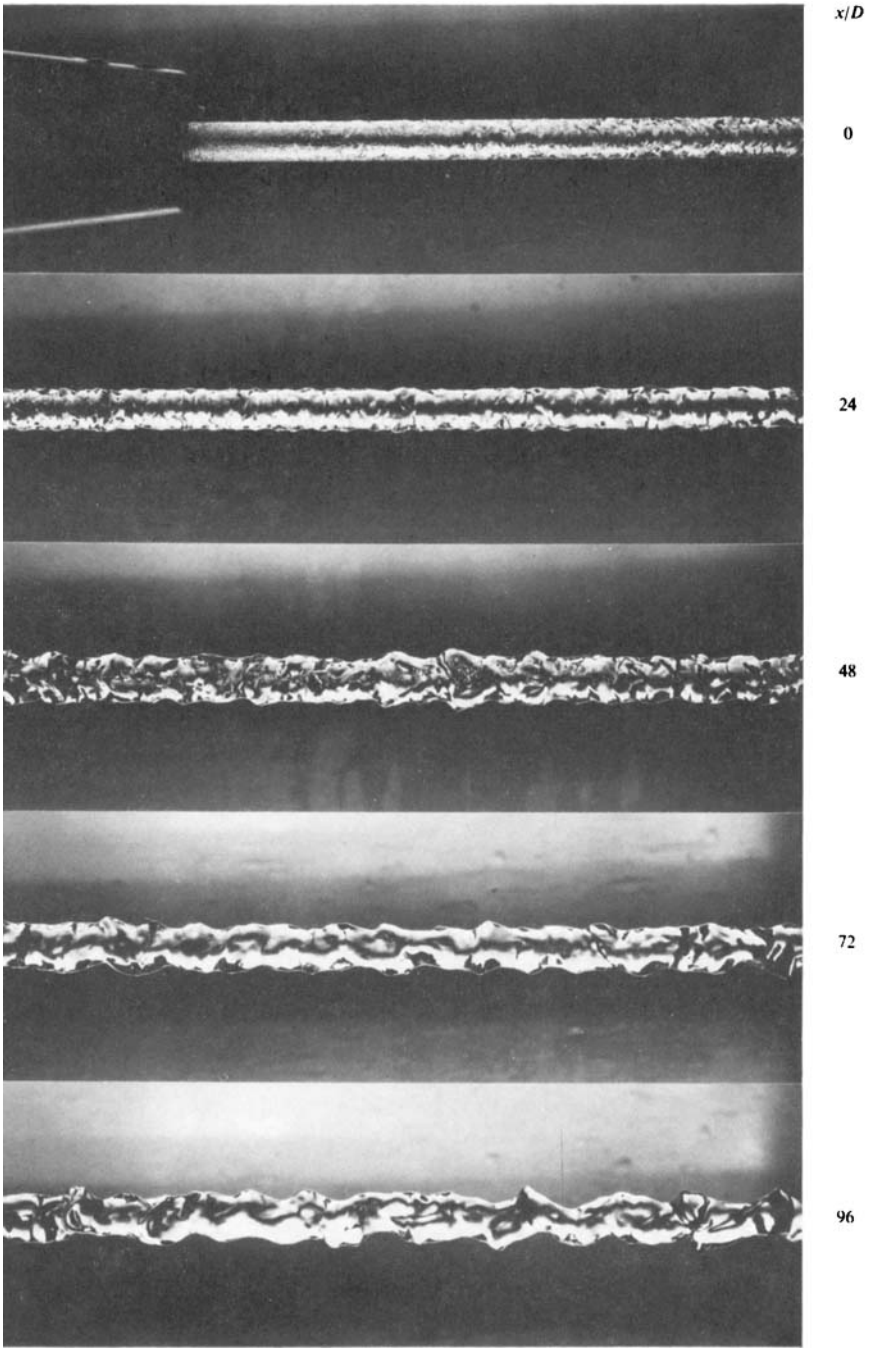

FIGURE 9 (*a*). For legend see facing page.

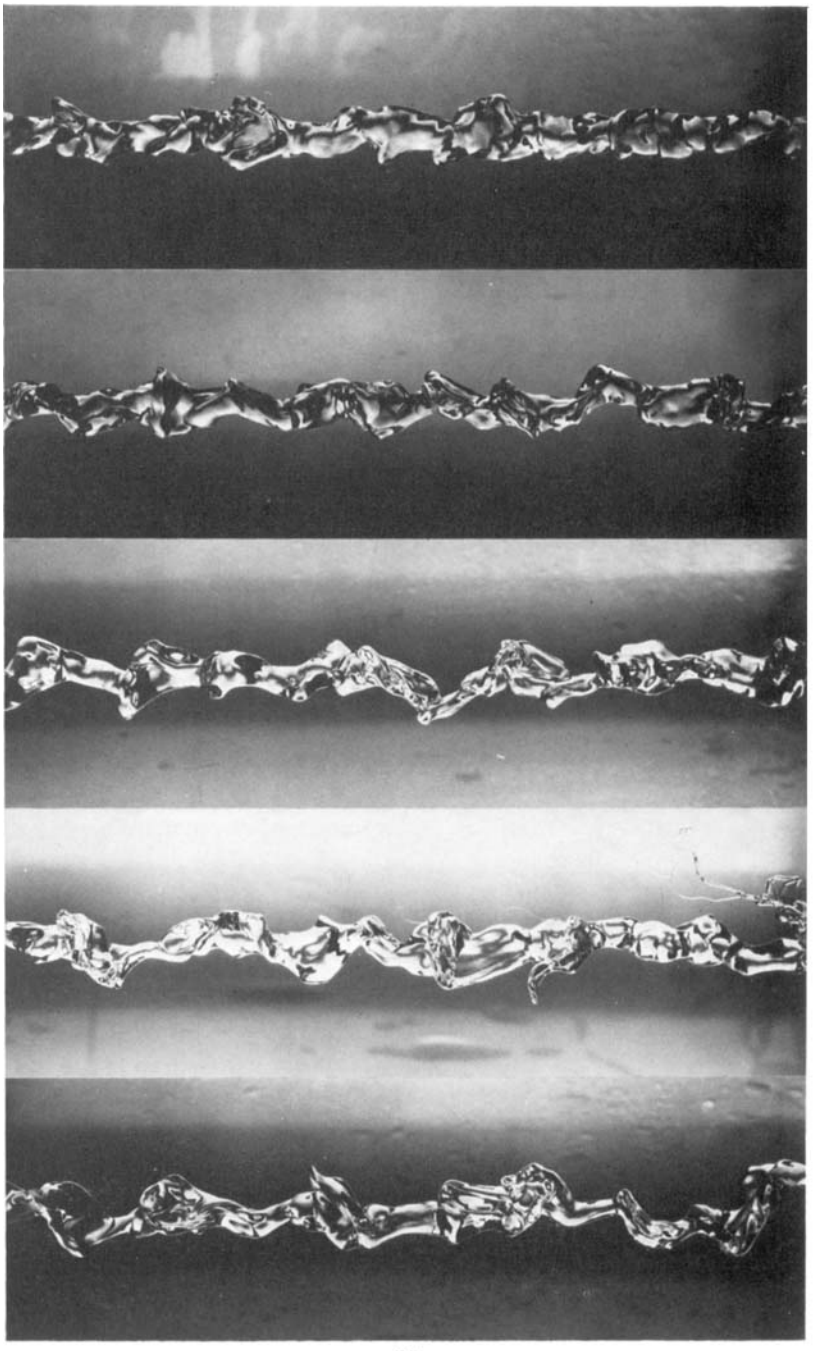

(*b*)

FIGURE 9. Photos of jet from 0·25 in. diameter nozzle in stagnant air using 200 p.p.m. poly-(ethylene oxide) solution instead of plain water; photos were taken 24 nozzle diameters apart.